JACS
JOURNAL OF THE AMERICAN CHEMICAL SOCIETY
Communication
pubs.acs.org/JACS

Titanium Nitride-Nickel Nanocomposite as Heterogeneous Catalyst for the Hydrogenolysis of Aryl Ethers

Valerio Molinari, Cristina Giordano, Markus Antonietti, and Davide Esposito*

Max-Planck-Institute of Colloids and Interfaces, 14424 Potsdam, Germany

Supporting Information

ABSTRACT: Lignin from biomass can become a sustainable source of aromatic compounds. Its depolymerization can be accomplished through hydrogenolysis, although the development of catalysts based on cheap and abundant metals is lacking. Herein, a sustainable composite based on titanium nitride and nickel is synthesized and employed as catalyst for the hydrogenolysis of aryl ethers as models for lignin. The catalytic activity of the new material during hydrogenation reactions is proven to be superior to that of either component alone. In particular, different aryl ethers could be efficiently converted under relatively mild conditions into aromatic compounds and cycloalkanes within minutes.

Lignin is the second most abundant biopolymer on earth after cellulose.[1] The development of strategies to depolymerize this complex molecule is gaining interest due to the possibility of obtaining aromatic platform chemicals from nonfossil resources.[2] However, this goal remains challenging due to the presence in the lignin structure of several ether and carbon−carbon bonds that are characterized by high energies and very different reactivities.[3] For instance, diaryl ethers are usually recalcitrant to react even under the severe conditions commonly applied during the hydrothermal, organosolv, or hydrolytic treatment of lignin.[4] To date, hydrogenolysis has been proposed to depolymerize lignin,[5] but the use of harsh conditions in combination with expensive and nonsustainable catalysts based on Ru, Rh, Pt, Pd was required.[5−8] Furthermore, the poor selectivity of these strategies leads often to the formation of mixtures of cycloalkanes and bio-oils that are difficult to process, while the isolation of pure aromatic compounds remains challenging. Nickel (Ni)-based catalysts are highly effective for hydrogenolysis reactions, and several research groups have been recently focused on investigating their properties encouraged by the availability and competitive price of Ni compared to other transition metals.[9] The group of Hartwig[10,11] recently reported an exciting protocol for the cleavage of aryl ethers under mild conditions in xylene based on a homogeneous Ni catalyst. Following this seminal work and considering the easier applicability of heterogeneous catalysts for industrial applications, other groups have investigated the possible use of heterogeneous Ni systems, including Raney Ni[12,13] and silica supported Ni.[14−16]

Among alternatives to noble metals, nitrides and carbides of early transition metals have been investigated as they exhibit similar properties to those of Pt-group metals,[17,18] but with the advantages of lower costs and higher availability. Catalytic applications of this class of metallic ceramics for oxidation,[19] reduction,[20] and alkylation[21] reactions have been recently reported. Interestingly, doping with Ni has been used as an approach to enhance the activity of tungsten carbides during the hydrogenation of cellulose to ethylene glycol.[20] More recently, tungsten carbides have been reported as efficient supports for the preparation of platinum-based electrocatalysts.[22] The role of semiconducting supports in heterogeneous catalysts and their ability to modify the electron density of the supported metal (Mott−Schottky effect) thereby modifying their activities has been recently highlighted.[23] In this work, titanium nitride (TiN) was used for the first time as support to enhance the catalytic activity of Ni. TiN is a biocompatible material[24,25] with excellent physical and chemical properties including thermal stability and acid resistance.[26,27] Its hybridization with Ni through a facile and scalable synthesis provided a noble metal-free nanocomposite characterized by high catalytic activity for the hydrogenolysis of aryl ethers, model molecules of lignin structure. A comparison of this material with pure TiN or Ni particles during hydrogenolysis was performed to elucidate the synergistic effect between the two components in the nanocomposite. We started with the synthesis of TiN nanoparticles by a reported urea route,[28] which involves the calcination under nitrogen flux of a titanium-urea gel-like precursor at 750 °C. The resulting powders presented a bronze color typical of TiN (Figure S1), whose formation was confirmed by XRD analysis (Figure 1). The addition of Ni (Ni/TiN ∼0.5 molar ratio) was performed in a second step, by impregnation of TiN with an ethanolic solution of Ni acetate tetrahydrate (NiAc), followed by solvent evaporation to give a bronze homogeneous powder (NiAc@TiN). Infrared analysis on NiAc@TiN showed an intense shift in the peak of the carbonyl group of the acetate compared to pure NiAc (Figure S2), diagnostic of an interaction with TiN. This powder was then calcined under nitrogen at different temperatures to obtain the composite material TiN-Ni. Figure 1 shows the XRD patterns of pure TiN-Ni nanocomposite obtained at 500 °C, together with the partially oxidized TiN-Ni obtained at 600 and 700 °C.

The oxidation of TiN at higher temperatures can be explained due to the presence of adsorbed oxygen (Figure S3, Table S1), which at elevated temperatures can promptly react with TiN. The oxophilicity of titanium is indeed well-known. Interestingly, pure TiN prepared via the urea route at

Received: November 22, 2013
Published: January 17, 2014

   dx.doi.org/10.1021/ja4119412 | J. Am. Chem. Soc. 2014, 136, 1758−1761

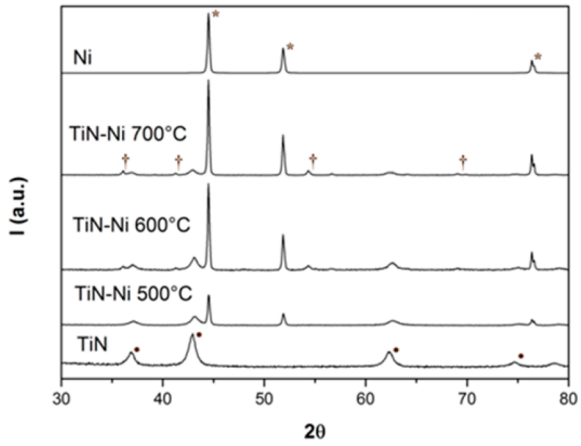

Figure 1. XRD patterns of TiN, Ni, and TiN-Ni at different temperatures. *: metallic Ni; †: TiO_2; ●: TiN.

higher temperature (up to 800 °C) has never shown TiOx as side products.[28] A shift (~ 0.5 θ) to higher angles in the TiN peak is observed in Figure 1 after Ni addition. A similar effect is observed in the patterns of Ni-titanates compounds.[29] Nevertheless, the presence of Ni-titanate and other possible side products like TiC was excluded by XRD analysis (Figure S6). To prove that the shift in the diffraction pattern of TiN is not caused by the secondary thermal treatment, fresh TiN was reheated at 500 °C without addition of Ni, and the resulting XRD pattern (Figure S7) remained unchanged. Interestingly, all attempts to prepare TiN-Ni in a one-pot procedure, by direct mixing of Ni precursors and the Ti@urea gel, afforded only TiO_2-Ni mixed phases (Figures S4, S5). In order to compare and understand the change in morphology and reactivity of the TiN-Ni nanocomposite, pure metallic Ni particles were also synthesized by carbothermal reduction of NiAc. The TEM images show small and monodisperse primary TiN nanoparticles (Figure 2A) and the TiN-Ni composite material (Figure 2B) obtained after Ni addition (see also Figure S8).

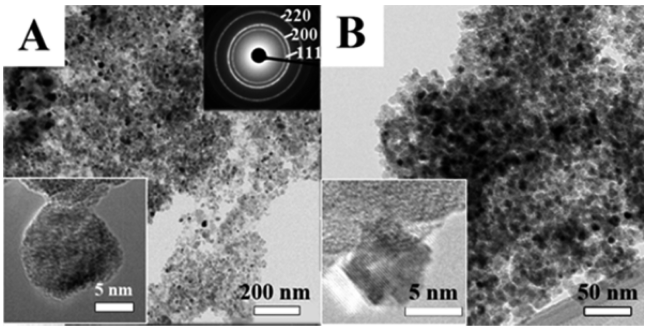

Figure 2. TEM pictures of (A) TiN and (B) TiN-Ni prepared at 500 °C.

As it can be deduced, the morphology of TiN nanoparticles was only slightly affected by the presence of Ni. The simultaneous presence of Ni and titanium in the final nanoparticles was confirmed by EDX investigation (see Figure S7). Interestingly, while titanium was always found together with Ni, few titanium-free areas could also be detected. Nitrogen sorption analysis was performed to estimate the surface area of Ni, TiN, and TiN-Ni (Figure S11). The change of morphology from small nanoparticles to an intergrown aggregate structure led to a decreased surface area of 116 m^2 g^{-1} for TiN-Ni compared to the initial 212 m^2 g^{-1} in TiN. This could be due to the higher density of the nanocomposites compared to pure TiN, caused by the presence of 50% Ni whose density is higher than the one of TiN (ρNi = 8.9 g cm^{-3}, ρTiN = 5.2 g cm^{-3}). On the other hand, these values may also reflect the increased agglomeration of the particles following Ni addition. Noteworthy, pure Ni particles showed a relatively lower surface area of ~30 m^2 g^{-1} and were characterized by a lower homogeneity, as deduced by SEM analysis (Figure S10).

In order to evaluate the catalytic activity of the obtained materials, the reduction of nitrobenzene to aniline in the presence of hydrogen has been studied as simple model reaction. All the catalytic tests were performed using a fixed bed flow reactor (H-Cube Pro) equipped with a packed cartridge of Ni, TiN, or TiN-Ni (500 °C) catalyst and provided with a gas (H_2) and a liquid feed. We commenced testing TiN for the hydrogenation reaction of nitrobenzene to aniline with temperatures ranging between 25 and 100 °C, but no conversion was observed even at high temperatures (Table S4, entry 1). Ni particles showed in turn moderate activity at 50 °C (entry 2), while good (80%) to high (>99%) conversions could be achieved at 75 and 100 °C, respectively (entries 3, 4). Interestingly, the improved activity of the TiN-Ni could be readily appreciated as full conversion was obtained at 25 °C (entry 5). These interesting preliminary results characterized Ni and TiN-Ni as promising hydrogenation catalysts.

Therefore, we went on testing the more challenging hydrogenolysis of aryl ethers. We focused our attention on model molecules that contain the most common aryl ether linkages found in lignin (Tables 1 and 2). Initially, we studied the hydrolysis of benzyl-phenyl ether **1** as a model for the α-O-4 linkage in lignin. In analogy to the reduction of nitrobenzene, hydrogenolysis of **1** in the presence of TiN as catalyst did not show detectable conversion (Table 1, entry 1). In contrast, Ni nanoparticles were effective in promoting this hydrogenolysis, and despite the low activity up to 125 °C, 90% conversion could be obtained at 150 °C (entries 3 and 4). Nevertheless, TiN-Ni composite showed a superior activity affording full conversion already at 125 °C (entry 6). GC analysis revealed the presence of phenol and toluene as the sole reaction products.

The cleavage of the alkyl aryl ether bond in phenylethyl phenyl ether **2** as a model for β-O-4 linkages in lignin occurred under more severe conditions, in line with its higher dissociation energy compared to **1**.[15] Once again, TiN showed no activity. Ni particles were also unable to promote conversion up to 150 °C. However, TiN-Ni catalyst presented a conversion of 65% at 150 °C with a flow rate of 0.5 mL min^{-1}, while full conversion could be achieved using a lower volumetric flow (0.3 mL min^{-1}) as can be seen in entries 9 and 10. In this case, chromatographic analysis revealed the formation of **5** and **7** as the sole products. Interestingly, **7** was not detected during the hydrogenolysis of **1** at 125 °C, while its formation becomes considerable at 150 °C, probably reflecting a faster hydrogenation rate for the phenol at this temperature.

Accordingly, control experiments on phenol **3** at 150 °C and 0.3 mL min^{-1} resulted in a conversion of 55% into **7**.

The 4-O-5 bond is one of the strongest ether bonds in lignin, and its hydrogenolysis was modeled using diphenyl ether **8** (Table 2). Unlike Ni and TiN (Table 2, entries 1, 2), TiN-Ni can successfully cleave diphenyl ether, and the best results

dx.doi.org/10.1021/ja4119412 | J. Am. Chem. Soc. 2014, 136, 1758−1761

Table 1. Effect of Ni, TiN, and TiN-Ni Catalysts on Hydrogenolysis of Different Lignin Model Molecules

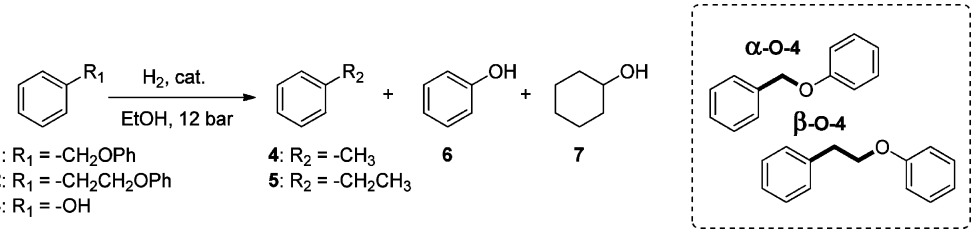

					selectivity (%)[c]				
entry	cat.	substrate	T (°C)	conversion (%)[c]	4	5	6	7	productivity (mmol h^{-1} g_{cat}^{-1})
1[a]	TiN	**1**	150	0	–	–	–	–	–
2[a]	Ni	**1**	100	0	–	–	–	–	–
3[a]	Ni	**1**	125	18	51	–	49	–	0.225
4[a]	Ni	**1**	150	90	57	–	43	–	1.282
5[a]	TiN-Ni	**1**	100	67	53	–	47	–	0.666
6[a]	TiN-Ni	**1**	125	>99	54	–	46	–	1.013
7[a]	TiN	**2**	150	0	–	–	–	–	–
8[b]	Ni	**2**	150	0	–	–	–	–	–
9[a]	TiN-Ni	**2**	150	65	–	57	–	43	0.695
10[b]	TiN-Ni	**2**	150	>99	–	54	–	46	0.608
11[b]	TiN-Ni	**3**	150	55	–	–	–	100	0.620

[a]Conditions: 0.05 M solution of starting material in EtOH, 12 bar, 0.5 mL min^{-1}. [b]0.3 mL min^{-1}. [c]Determined by GC-MS analysis.

Table 2. Effect of Ni, TiN, and TiN-Ni Catalysts on Hydrogenolysis of Different Diaryl Ethers

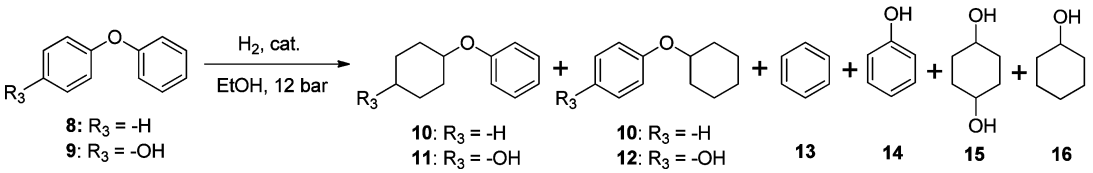

					selectivity (%)[c]							
entry	cat.	substrate	T (°C)	conversion[c] (%)	10	11	12	13	14	15	16	productivity (mmol h^{-1} g_{cat}^{-1})
1[a]	TiN	**8**	150	0	–	–	–	–	–	–	–	–
2[a]	Ni	**8**	150	<5	–	–	–	–	–	–	–	–
3[a]	TiN-Ni	**8**	125	68	42	–	–	35	–	–	23	0.223
4[b]	TiN-Ni	**8**	150	99	5	–	–	46	–	–	49	0.259
5[b,d]	TiN-Ni	**9**	150	65	–	22	–	49	–	25	4	0.179

[a]Conditions: 0.025 M of starting material in EtOH, 12 bar, 0.5 mL min^{-1}. [b]0.3 mL min^{-1}. [c]Determined by GC-MS analysis. [d]Uncorrected GC data.

could be obtained at 150 °C and 0.3 mL min^{-1} volumetric flow, with a feed concentration of 25 mM (entry 4). Interestingly, during hydrogenolysis of compound **8** we observed the formation of **10** at low conversion (entry 3). In contrast, traces of **10** were observed at 150 °C (entry 4), leading to the conclusion that, at this temperature, dearomatization does not compete with C−O cleavage. A comparison of the selectivity for the hydrogenolysis of compound **8** at full conversion proved TiN-Ni highly competitive with respect to representative commercial hydrogenation catalysts, including Pd/C and Raney Ni (Table S5). To investigate a possible selectivity in the hydrogenolysis of substituted 4-O-5 linkages, compound **9** was also hydrogenated using the conditions optimized for compound **8** (entry 5). According to GC analysis, the mixture of products is mostly composed of benzene and 1,4 cyclohexanediol revealing a preference of the catalyst to promote the cleavage of the C−O bond associated with the most electron-deficient phenyl unit.

Having proved the applicability of the catalyst to the cleavage of different aryl ethers, we performed a qualitative evaluation of its stability vs time on stream. The efficiency of the particles was tested up to ∼40 h of reaction at 150 °C and remained unaffected. Also structural features remained unchanged as confirmed by XRD (Figure S12) performed after catalyst utilization. A preliminary and qualitative hydrogenolysis test on commercial lignin samples under nonoptimized conditions showed the formation of an array of low molecular weight aromatic and aliphatic products (Figure S14) anticipating the possible application of the catalysts for depolymerization of real lignin samples. Noteworthy, the use of this new nanocomposite in combination with a fixed bed reactor resulted particularly effective in achieving high productivities. Considering a void volume of 0.5−0.8 mL for the catalyst bed and a flow rate of 0.3 mL min^{-1}, high conversions could be obtained with very short residence times (1.5−2.6 min) with respect to previously published data.[11,15] Although additional insights will be required in order to understand the improved activity of the new composites with respect to pure Ni, a speculative interpretation of the physochemical effects operating in the catalysts can be done on the basis of the observed results. The

dx.doi.org/10.1021/ja4119412 | J. Am. Chem. Soc. 2014, 136, 1758−1761

partial oxidation of TiN in the nanohybrid at elevated temperatures (Figure 1), together with the oxidative stability of Ni, suggests an electron transfer from the Ni to the TiN. As both component are metals and structurally tightly bonded, electrons will flow from the less noble (Ni) to the more noble (TiN) side of the composite in order to equilibrate the Fermi levels.[23] The resulting electron-deficient Ni, for instance, might more effectively coordinate the oxygen of ether linkages and activate them for hydrogenation, while accelerating the hydride transfer to the arene during reductive elimination. Nevertheless, a classical binary catalysis scheme in which ether linkages are activated by available Ti-coordination sites on the TiN substructure and hydrogen is activated by Ni cannot be excluded. Finally, a possible templating effect in which TiN could favor the formation of Ni particles with optimal morphology and site density remains to be elucidated. A more detailed reaction mechanism will be provided on the basis of additional studies.

In conclusion, we introduced a new TiN-Ni nanocomposite composed of spherical intergrown core−shell nanoparticles of ∼10 nm in diameter, as estimated both via XRD and HR-TEM. This novel material was synthesized on a multigram scale and proved to be stable at room temperature both in air and in solvent for several months. The close contact between TiN and Ni was observed both via peak position and intensity changes in the corresponding XRD pattern. Furthermore, a different chemical behavior and catalytic activity was observed with respect to pure Ni and TiN. While simple Ni particles were found to be less efficient for the reductive splitting or hydrogenolysis of lignin model molecules, a superior catalytic activity of the TiN-Ni nanocomposite was shown, even with the very recalcitrant diphenyl ether linkages.

The nanocomposite worked as an efficient catalyst in a fixed bed reactor, and using ethanol as an environmentally benign solvent afforded high conversions in very short reaction times. These promising results open the way to new competitive lignin refining strategies based on relatively cheap and abundant materials like Ti and Ni. A detailed investigation of the reaction mechanism including the influence of other solvents will be the subject of future studies. Finally, this work anticipates the development of an extended family of new catalysts, whose activity is based on the interaction of early transition-metal nitrides with Ni, which can find application in different fields of catalysis.

■ ASSOCIATED CONTENT

Supporting Information

Additional experimental and characterization details. This material is available free of charge via the Internet at http://pubs.acs.org.

■ AUTHOR INFORMATION

Corresponding Author

Davide.Esposito@mpikg.mpg.de

Notes

The authors declare no competing financial interest.

■ ACKNOWLEDGMENTS

We gratefully thank Dr. Guylhaine Clavel for TEM measurements and fruitful discussion and the Max Planck-Fraunhofer cooperation scheme for financial support.

■ REFERENCES

(1) Boerjan, W.; Ralph, J.; Baucher, M. *Annu. Rev. Plant Biol.* **2003**, *54*, 519.
(2) Marshall, A.-L.; Alaimo, P. J. *Chem.—Eur. J.* **2010**, *16*, 4970.
(3) Wang, X.; Rinaldi, R. *ChemSusChem* **2012**, *5*, 1455.
(4) Laskar, D. D.; Yang, B.; Wang, H.; Lee, J. *Biofuels, Bioprod. Biorefin.* **2013**, *7*, 602.
(5) Zakzeski, J.; Bruijnincx, P. C. A.; Jongerius, A. L.; Weckhuysen, B. M. *Chem. Rev.* **2010**, *110*, 3552.
(6) Michael Robinson, J.; E. Burgess, C.; A. Bently, M.; D. Brasher, C.; O. Horne, B.; M. Lillard, D.; M. Macias, J.; D. Mandal, H.; C. Mills, S.; D. O'Hara, K.; T. Pon, J.; F. Raigoza, A.; H. Sanchez, E.; Villarreal, S. *J. Biomass Bioenergy* **2004**, *26*, 473.
(7) Pepper, J. M.; Hibbert, H. *J. Am. Chem. Soc.* **1948**, *70*, 67.
(8) Pepper, J. M.; Lee, Y. W. *Can. J. Chem.* **1969**, *47*, 723.
(9) Alonso, F.; Riente, P.; Yus, M. *Acc. Chem. Res.* **2011**, *44*, 379.
(10) Sergeev, A. G.; Hartwig, J. F. *Science* **2011**, *332*, 439.
(11) Sergeev, A. G.; Webb, J. D.; Hartwig, J. F. *J. Am. Chem. Soc.* **2012**, *134*, 20226.
(12) Wang, X. Y.; Rinaldi, R. *Energy Environ. Sci.* **2012**, *5*, 8244.
(13) Wang, X.; Rinaldi, R. *Angew. Chem., Int. Ed.* **2013**, *52*, 11499.
(14) Toledano, A.; Serrano, L.; Balu, A. M.; Luque, R.; Pineda, A.; Labidi, J. *ChemSusChem* **2013**, *6*, 529.
(15) He, J.; Zhao, C.; Lercher, J. A. *J. Am. Chem. Soc.* **2012**, *134*, 20768.
(16) Toledano, A.; Serrano, L.; Labidi, J.; Pineda, A.; Balu, A. M.; Luque, R. *ChemCatChem* **2013**, *5*, 977.
(17) Levy, R. B.; Boudart, M. *Science* **1973**, *181*, 547.
(18) Hwu, H. H.; Chen, J. G. *Chem. Rev.* **2004**, *105*, 185.
(19) Villa, A.; Campisi, S.; Giordano, C.; Otte, K.; Prati, L. *ACS Catal.* **2012**, *2*, 1377.
(20) Ji, N.; Zhang, T.; Zheng, M.; Wang, A.; Wang, H.; Wang, X.; Chen, J. G. *Angew. Chem., Int. Ed.* **2008**, *47*, 8510.
(21) Yao, W.; Makowski, P.; Giordano, C.; Goettmann, F. *Chem.—Eur. J.* **2009**, *15*, 11999.
(22) Esposito, D. V.; Hunt, S. T.; Kimmel, Y. C.; Chen, J. G. *J. Am. Chem. Soc.* **2012**, *134*, 3025.
(23) Li, X.-H.; Antonietti, M. *Chem. Soc. Rev.* **2013**, *42*, 6593.
(24) Hämmerle, H.; Kobuch, K.; Kohler, K.; Nisch, W.; Sachs, H.; Stelzle, M. *Biomaterials* **2002**, *23*, 797.
(25) Birkholz, M.; Ehwald, K. E.; Wolansky, D.; Costina, I.; Baristiran-Kaynak, C.; Fröhlich, M.; Beyer, H.; Kapp, A.; Lisdat, F. *Surf. Coat. Technol.* **2010**, *204*, 2055.
(26) Heide, N.; Schultze, J. W. *Nucl. Instrum. Methods Phys. Res., Sect. B* **1993**, *80−81* (Part1), 467.
(27) Marlo, M.; Milman, V. *Phys. Rev. B* **2000**, *62*, 2899.
(28) Giordano, C.; Erpen, C.; Yao, W.; Milke, B.; Antonietti, M. *Chem. Mater.* **2009**, *21*, 5136.
(29) pattern of Ni-titanates can be found under http://www.icdd.com.